Cell Reports
Report

Structural Basis of SOSS1 Complex Assembly and Recognition of ssDNA

Wendan Ren,[1,2,4] Hongxia Chen,[1,4] Qiangzu Sun,[1,4] Xuhua Tang,[2] Siew Choo Lim,[2] Jun Huang,[1,*] and Haiwei Song[1,2,3,*]
[1]Life Sciences Institute, Zhejiang University, 388 Yuhangtang Road, Hangzhou 310058, China
[2]Institute of Molecular and Cell Biology, 61 Biopolis Drive, Singapore 138673, Singapore
[3]Department of Biochemistry, National University of Singapore, 14 Science Drive, Singapore 117543, Singapore
[4]These authors contributed equally to this work
*Correspondence: jhuang@zju.edu.cn (J.H.), haiwei@imcb.a-star.edu.sg (H.S.)
http://dx.doi.org/10.1016/j.celrep.2014.02.020

SUMMARY

The SOSS1 complex comprising SOSSA, SOSSB1, and SOSSC senses single-stranded DNA (ssDNA) and promotes repair of DNA double-strand breaks (DSBs). But how SOSS1 is assembled and recognizes ssDNA remains elusive. The crystal structure of the N-terminal half of SOSSA ($SOSSA_N$) in complex with SOSSB1 and SOSSC showed that $SOSSA_N$ serves as a scaffold to bind both SOSSB1 and SOSSC for assembly of the SOSS1 complex. The structures of $SOSSA_N$/B1 in complex with a 12 nt ssDNA and $SOSSA_N$/B1/C in complex with a 35 nt ssDNA showed that SOSSB1 interacts with both $SOSSA_N$ and ssDNA via two distinct surfaces. Recognition of ssDNA with a length of up to nine nucleotides is mediated solely by SOSSB1, whereas neither SOSSC nor $SOSSA_N$ are critical for ssDNA binding. These results reveal the structural basis of SOSS1 assembly and provide a framework for further study of the mechanism governing longer ssDNA recognition by the SOSS1 complex during DSB repair.

INTRODUCTION

The integrity of genomic DNA is constantly challenged by a variety of endogenous and exogenous DNA damaging agents such as replication fork collapse, oxidative stress, and ionizing radiation (IR) to induce DNA double-strand breaks (DSBs) (Aguilera and Gómez-González, 2008). DSBs are highly toxic and can cause genome rearrangement and cell death. Defective DSB repair can cause genome instability and disease, including developmental disorders, premature aging, and cancer predisposition (Jackson and Bartek, 2009; McKinnon, 2009). Eukaryotic cells have evolved two primary pathways to repair DNA DSBs: nonhomologous end joining (NHEJ) and homologous recombination (HR) (Symington and Gautier, 2011). The choice between these two pathways depends on the nature of DSB and the phase of cell cycle (Bartek et al., 2004; Sonoda et al., 2006). One of the initial steps in the process of HR is the resection of DSBs to generate a 3′-single-stranded DNA (ssDNA) overhang, which is essential for Rad51-mediated strand exchange (D'Amours and Jackson, 2002; Jazayeri et al., 2008; Lee and Paull, 2005).

Single-stranded-DNA-binding proteins (SSBs) play essential roles in DNA replication, recombination, DNA damage signaling, and repair in bacteria, archaea, and eukarya (Shereda et al., 2008). A hallmark of these proteins is that they possess oligonucleotide/oligosaccharide binding folds (OB folds) that bind ssDNA or ssRNA (Flynn and Zou, 2010; Murzin, 1993). The human SSB, known as human replication protein A (RPA), is a stable heterotrimer composed of three subunits RPA70, RPA32, and RPA14 (also named as RPA1, RPA2, and RPA3) that are conserved among eukaryotes (Iftode et al., 1999; Wold, 1997). RPA is generally believed to be the major SSB protein in eukaryotic cells given that it is not only critically important for DNA replication, but also participates in various DNA repair and recombination processes (Zou et al., 2006). Recently, two additional ssDNA-binding proteins hSSB1 and hSSB2 have been identified in the human genome (Richard et al., 2008). Both proteins contain a single highly conserved OB fold, a divergent spacer domain followed by a conserved C-terminal tail predicted to be involved in protein-protein interactions. Following IR-induced DNA damage, hSSB1 is stabilized by ATM-dependent phosphorylation and localizes to the sites of damaged DNA as discrete foci (Richard et al., 2008). Cells depleted of either hSSB1 or hSSB2 cause checkpoint defects, reduced HR, and increased radiosensitivity, suggesting that both proteins are required for proper repair of damaged DNA (Richard et al., 2008). In addition to its role in DNA repair, hSSB1 regulates both the stability and the transcriptional activity of p53 (Xu et al., 2013) and also binds and protects p21 from ubiquitin-mediated degradation (Xu et al., 2011). Mouse SSB1 and SSB2 have also been shown to protect newly replicated telomeres (Gu et al., 2013).

Recently, we (Huang et al., 2009) and other groups (Li et al., 2009; Skaar et al., 2009) have demonstrated that hSSB1 and hSSB2 function at DSBs to form two separate heterotrimeric complexes with INTS3 and C9orf80, termed sensor of single-stranded DNA complex 1 and 2 (SOSS1/2). Accordingly, INTS3, hSSB1/2, and C9orf80 were designated as SOSS subunit A, B1/2, and C, respectively (Huang et al., 2009). SOSSA serves as a central adaptor required not only for SOSS complex

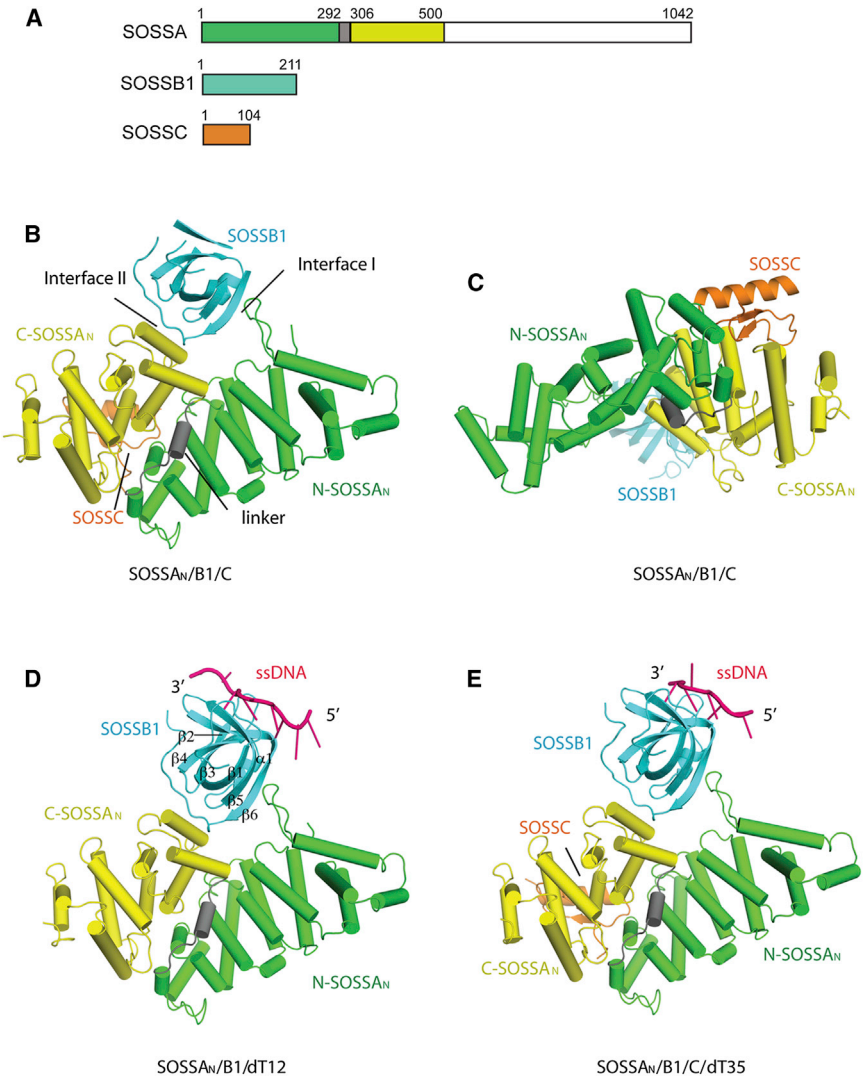

Figure 1. Structures of the SOSS 1 Complex in Isolation and in Complex with ssDNA

(A) Schematic representation of the domain organization in SOSSA, SOSSB1, and SOSSC.

(B) Structure of the SOSSA$_N$/B1/C complex.

(C) Structure of the SOSSA$_N$/B1/C complex with the orientation relative to (B) rotated along y axis by 180° then along x axis by 270°.

(D) Structure of SOSSA$_N$/B1 complexed with dT12.

(E) Structure of SOSSA$_N$/B1/C complexed with dT35. For (B), (D), and (E), structures are superimposed at SOSSA$_N$ to make sure that the orientations are identical. The N-terminal, linker, and C-terminal regions of SOSSA$_N$ are colored in green, gray, and yellow-green, respectively. SOSSB1 and SOSSC are in cyan and orange, respectively. The bound ssDNA is shown in pink.

assembly and stability, but also for facilitating the accumulation of SOSS complex to the sites of DNA damage (Huang et al., 2009; Li et al., 2009). Moreover, similar to depletion of hSSB1, silencing of SOSSA and SOSSC displays increased ionizing radiation sensitivity, defective G2/M checkpoint, and impaired HR repair (Huang et al., 2009; Li et al., 2009; Skaar et al., 2009; Zhang et al., 2009).

Like RPA, recombinant human SSB1 binds specifically to ssDNA, and the binding affinity increases significantly with the length of the ssDNA substrate (Richard et al., 2008). Most recently, the DNA-binding properties of the SOSS1 complex were compared with those of RPA using ensemble and single-molecule approaches (Yang et al., 2013). Compared to RPA, SOSS1 binds to ssDNA with lower affinity and exhibits less stable and dynamic interactions with the ssDNA substrate. The binding of the SOSS1 complex to ssDNA promotes DNA end resection in concert with human Exonuclease 1 (hExo1) (Yang et al., 2013), an enzyme critical for DNA resection in eukaryotes (Tran et al., 2004).

To gain insights into the molecular basis of the SOSS1 complex assembly and its recognition for ssDNA, we reconstituted a SOSS1 subcomplex containing the N-terminal half of SOSSA (SOSSA$_N$) and full-length SOSSB1 (designated as SOSSA$_N$/B1), and a trimeric complex composed of SOSSA$_N$/B1 and full-length SOSSC (designated as SOSSA$_N$/B1/C). We then determined the crystal structures of SOSSA$_N$/B1/C in apo form and in complex with a 35 nt ssDNA as well as the structure of SOSSA$_N$/B1 in complex with a 12 nt ssDNA. These structures combined with functional analysis confirmed that SOSSA acts as a scaffold to bridge the interaction between SOSSB1 and SOSSC and showed that the OB fold domain of SOSSB1 binds to SOSSA and ssDNA through two distinct surfaces. The OB fold domain of SOSSB1 is solely responsible for the recognition of a short ssDNA (up to nine nucleotides), whereas SOSSA$_N$ and SOSSC are not essential for ssDNA binding. These results reveal the structural basis of the SOSS1 complex assembly and serve as a cornerstone for further elucidating the mechanism underlying longer ssDNA recognition by SOSS1 during resection of DSBs.

RESULTS

Overall Structure of the SOSSA$_N$/B1/C Complex

The crystal structure of the human SOSSA$_N$/B1/C complex comprising the N-terminal half of SOSSA (SOSSA$_N$; residues 1–500), full-length SOSSB1 (residues 1–211), and full-length SOSSC (residues 1–104) (Figure 1A) was solved using single-wavelength anomalous dispersion (SAD) method. The structure was further built and refined at a resolution of 2.0 Å to working and free R factors of 17.19% and 19.53%, respectively. There is one SOSSA$_N$/B1/C complex in the asymmetric unit consisting

of one copy of each subunit. Several regions of the polypeptide chains are disordered, namely, residues 1–32 and 499–500 in $SOSSA_N$, residues 1–4, 11–18, 28–37, 71–81, 87–90, and 110–211 in SOSSB1, and residues 1–62 and 102–104 in SOSSC.

$SOSSA_N$ adopts an all α-helical fold that can be separated into two domains, N-$SOSSA_N$ (residues 33–292) and C-$SOSSA_N$ (residues 306–498), which are linked by an extended stretch of peptide (residues 293–305) containing a small α helix (α16) in the middle (Figures 1B and 1C). These two domains interact each other through direct and the linker region mediated contacts, forming a deep C-shaped cavity (~20 Å in depth) that clamps SOSSB1 tightly. On the opposite side of $SOSSA_N$, the two domains form a shallow groove for SOSSC to bind. A search of homologous structures for each domain using the DALI server (Holm and Rosenström, 2010) indicated that N-$SOSSA_N$ structurally resembles the middle domain of eukaryotic initiation factor 4F subunit G (eIF4G, PDB code: 2vso) with a *Z* score of 11.1 and an rmsd value of 4.3 Å for 179 Cα atoms (Figure S1). The best structural homolog for C-$SOSSA_N$ is the middle domain of human polyadenylate-binding protein-interacting protein 1 (Paip1, PDB code: 3rk6) (*Z* score: 7.4; rmsd: 3.7 Å for 144 Cα atoms), which is also structurally homologous to eIF4G (Lei et al., 2011) (Figure S1). eIF4G is a scaffold protein that links eIF4A and eIF4E together to form the eIF4F complex that is critical for translation initiation (Morino et al., 2000). The structural similarity between $SOSSA_N$ and eIF4G, together with the observation that $SOSSA_N$ interacts with both SOSSB1 and SOSSC, confirms the previous observations that SOSSA indeed serves as a scaffold for the SOSS1 assembly and the N-terminal 500 amino acids are necessary and sufficient for its interaction with SOSSB1 and SOSSC (Huang et al., 2009; Li et al., 2009; Skaar et al., 2009; Zhang et al., 2009).

SOSSB1 contains a single OB domain. As shown in Figure 1B, the polypeptide chain of residues 5–109 adopts a typical OB fold with five β strands (β1, β3, β4, β5, and β6) forming a curved beta barrel, which is capped by a short α helix (α1) between β4 and β5. Besides that, SOSSB1 has an extra small β strand (β2), which is antiparalleled to β3. The OB fold of SOSSB1 is highly similar to other single-stranded DNA binding proteins (SSBs) despite weak sequence similarity (less than 20% similarity). The best match is the SSB protein from *sulfolobus solfataricus* with a Z score of 14.5 (Kerr et al., 2003) followed by the replication protein A (RPA) from *Methanococcus maripaludis* with a Z score of 12.7 (PDB code: 3E0E). SOSSB1 binds to $SOSSA_N$ exclusively through its OB fold (Figure 1B). SOSSC folds into a long α helix followed by a two-stranded antiparalleled β sheet with the β sheet exclusively mediating its interaction with $SOSSA_N$ (Figure 1C). Consistent with the previous binding analysis (Huang et al., 2009), there is no direct interaction between SOSSB1 and SOSSC.

The SOSSA/SOSSB1 Interface

The structure of $SOSSA_N$/B1/C reveals that SOSSA interacts with SOSSB1 extensively with a buried accessible surface area of 1,740 $Å^2$. Two major contact areas are found in the interface between SOSSA and SOSSB1. In the C-shaped cavity (Figure 1B), the N-terminal tail of SOSSA interacts with helix $α1_B$ and strand $β6_B$ of SOSSB1 to create one contact area (interface I), whereas $α17_A$ and $α18_A$ and the loop connecting them in SOSSA interact with strand $β1_B$, the $α1_B$-$β5_B$ loop and the C-terminal tail (residues 97–102) of SOSSB1 to generate the second contact area (interface II; the subscript letters represent the subunit's name).

In both contact areas, hydrophobic interactions are predominant forces in mediating the interactions between SOSSA and SOSSB1 (Figures 2A and 2B). Specifically, residues $Phe315_A$, $Tyr328_A$, $Trp331_A$ of SOSSA form a hydrophobic groove to interact with a hydrophobic patch formed by residues $Ile22_B$, $Pro64_B$, $Phe98_B$, $Val101_B$, and $Tyr102_B$ of SOSSB1. Additional hydrophobic interactions involve residues $Thr40_A$ and $Leu42_A$ from the N terminus of SOSSA and $Leu61_B$ and $Ile62_B$ from $α1_B$ of SOSSB1. In addition to these predominant hydrophobic interactions, $Lys312_A$ of SOSSA forms a salt bridge with $Glu97_B$ of SOSSB1, whereas $Arg327_A$ contacts $Glu104_B$ via charge-charge interactions. Moreover, the side chains of $Arg327_A$ and $Trp331_A$ are hydrogen bonded to the main-chain carbonyl group of $Leu24_B$ and the main-chain amide group of $Gly65_B$, respectively. Both $Leu42_A$ and $Ala44_A$ interact with $Lys94_B$ via backbone-backbone hydrogen bondings. The residues involved in the SOSSA/SOSSB1 interface are strongly conserved in eukaryotes (Figure S2).

The SOSSA/SOSSC Interface

The interaction of SOSSA and SOSSC involves a concave surface formed by helices $α13_A$, $α14_A$, $α21_A$, and $α23_A$ of SOSSA and strands $β1_C$, $β2_C$ and loops $α1_C$-$β1_C$, $β1_C$-$β2_C$ and the C terminus excepting the N-terminal helix $α1_C$ in SOSSC (Figure 2C). The interaction of SOSSA and SOSSC is mainly mediated by hydrogen bonds with a buried accessible surface area of 2,470 $Å^2$. Specifically, $Gln259_A$ and $Phe444_A$ of SOSSA interact with $Tyr82_C$ and $Leu98_C$ of SOSSC, respectively, via backbone-backbone hydrogen bondings. Similarly, the main-chain amide groups of $Ala262_A$ and $Arg263_A$ of SOSSA form hydrogen bonds with the backbone carbonyl group of $Ser80_C$ of SOSSC, which in turn is hydrogen bonded via its side chain to the backbone carbonyl group of $Asn260_A$. Moreover, $Lys392_A$, $Thr432_A$, and $Asp435_A$ of SOSSA interact with $Asn92_C$ of SOSSC through hydrogen bonding between their side chains, whereas $Arg439_A$ of SOSSA makes multiple contacts with $Gln86_C$, $Asp87_C$, and $Ser88_C$ of SOSSC through charge-charge and hydrogen-bonding interactions. All the residues involved in the SOSSA/SOSSC interface are invariant among eukaryotic species except in zebrafish where $Tyr82_C$ of SOSSC is replaced by a phenylalanine (Figure S2).

Mutational Analyses of the SOSS1 Subunit Interfaces

To identify the residues important for the assembly of the SOSS1 complex, we mutated residues in the interfaces of SOSSA/SOSSB1 and SOSSA/SOSSC and examined the binding of these mutants to their respective wild-type binding partners using coimmunoprecipitation. Mutation of either Leu42 or Asp435 to Ala in SOSSA abolished its binding to SOSSB1 and SOSSC, respectively, whereas the R439A mutant of SOSSA showed substantially reduced binding to SOSSC (Figure 2D). Similarly, all three single mutants E97A, F98A, and E104A in SOSSB1 exhibited either residual or no binding at all to SOSSA

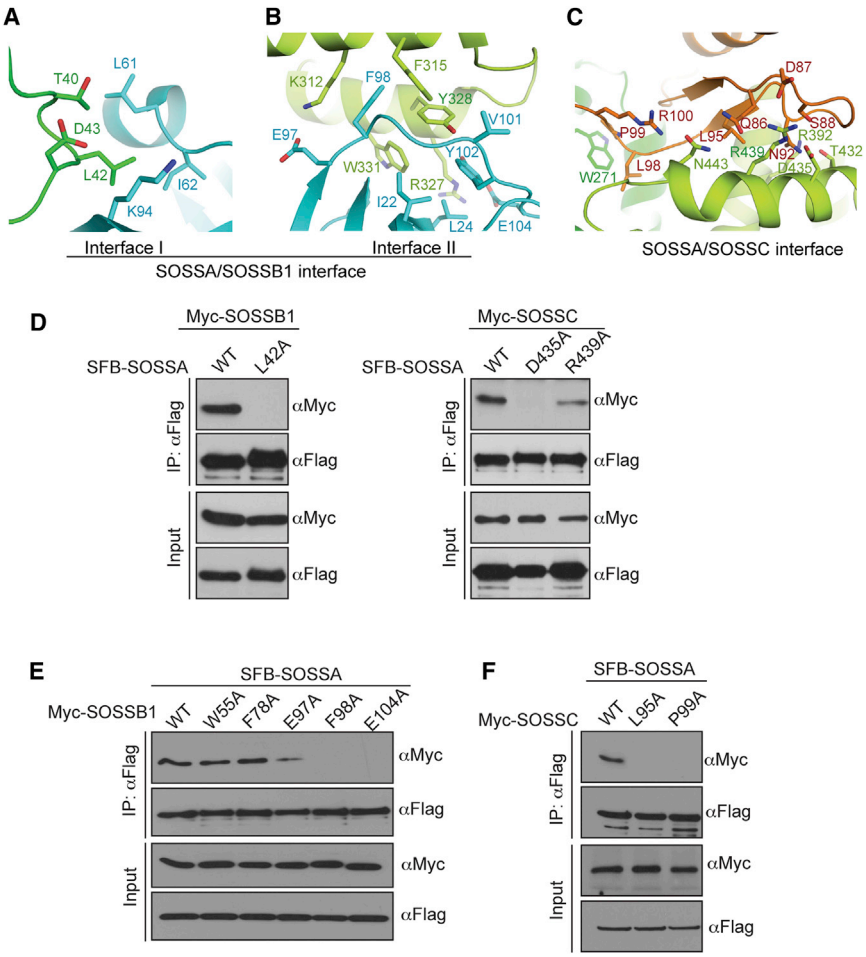

Figure 2. The Interfaces of the SOSSA$_N$/B1/C Complex

(A) The first interaction area includes N-terminal loop of SOSSA and the helix α1 strand β6 of SOSSB1.

(B) The second interface involves α17 and α18 of SOSSA and the α1-β5 loop strand β1 as well as C-terminal tail of SOSSB1.

(C) The interface between SOSSA and SOSSC includes loop α13-α14, helices α14, α23 of SOSSA, and strands β1 and β2 as well as the loop β1-β2 of SOSSC. The color scheme for individual subunits is as in Figure 1. The key residues of the interfaces are shown in stick and labeled.

(D) The L42A, D435A, and R439A mutants of SOSSA fail to interact with SOSSB1 and SOSSC, respectively. 293T cells were transiently transfected with plasmids encoding Myc-tagged SOSSB1 or SOSSC together with plasmids encoding SFB-tagged wild-type SOSSA or its point mutants. Cell lysates were immunoprecipitated with anti-Flag antibody, and western blot analysis was performed with anti-Flag and anti-Myc antibodies.

(E) The E97A, F98A, and E104A mutants of SOSSB1 fail to interact with SOSSA. 293T cells were transiently transfected with plasmids encoding SFB-tagged SOSSA together with plasmids encoding Myc-tagged wild-type SOSSC or its point mutants. Cell lysates were immunoprecipitated with anti-Flag antibody, and western blot analysis was performed with anti-Flag and anti-Myc antibodies.

(F) The L95A and P99A mutants of SOSSC fail to interact with SOSSA. Coimmunoprecipitation experiments were performed similar to those described in (D).

(Figure 2E), whereas both of the two mutants L95A and P99A in SOSSC failed to interact with SOSSA (Figure 2F). Consistent with this finding, the mutant F98A of mouse SOSSB1 (corresponding to human F98A) has been shown to lose its ability to bind SOSSA (Gu et al., 2013). Altogether, these mutagenesis results show that these residues are indeed important for the assembly of the SOSS1 complex in the context of the full-length proteins in vivo, consistent with our structural analysis.

Cells deficient in any component of the SOSS1 complex have been shown to display increased IR sensitivity and defective HR repair (Huang et al., 2009; Li et al., 2009; Skaar et al., 2009; Zhang et al., 2009). To explore whether the SOSS1 complex formation is required for proper cellular response to DNA damage, we took advantage of the inducible expression system to express the small interfering RNA (siRNA)-resistant wild-type SOSSA, SOSSB1, SOSSC, and their mutants defective in SOSS1 complex formation. As shown in Figures 3A–3C, the expression of wild-type and mutated SOSS1 subunits was induced when cells were treated with doxycycline. Interestingly, the expression level of the SOSSB1 mutants and the SOSSC mutants, but not the SOSSA mutants, is significantly lower than that of wild-type (Figures 3A–3C). These findings are in line with our previous observation that SOSSA is required for the stability of SOSSB1 and SOSSC, but not vice versa (Huang et al., 2009). In addition, wild-type SOSSA, SOSSB1, and SOSSC were distributed in the nucleus, whereas the SOSSB1 mutants and the SOSSC mutants, but not the SOSSA mutants, displayed a diffused cytoplasmic localization (Figures 3D–3F). These results suggest that SOSSA promotes SOSSB1 and SOSSC nuclear localization. More importantly, wild-type SOSS1 subunits successfully restored RAD51 focus formation to the levels comparable to that of control cells, whereas their mutants defective in SOSS1 complex formation failed to do so (Figures 4A–4C and S3). Consistently, reconstitution with wild-type SOSS1 subunits, but not their mutants, restored cell survival after IR treatment (Figures 4D–4F). Taken together, these results indicated that the assembly of the SOSS1 complex is required for proper repair of the damaged DNA.

SOSSB1 Interacts with SOSSA and ssDNA via Distinct Surfaces

To gain insights into how the SOSS1 complex interacts with ssDNA, we solved the crystal structure of SOSSA$_N$/B1 in complex with a 12 nucleotide poly(dT) (designated as SOSSA$_N$/B1/dT12). Although a 12 nucleotide ssDNA (dT12) was used in crystallization, we only observed nine deoxythymide nucleotides

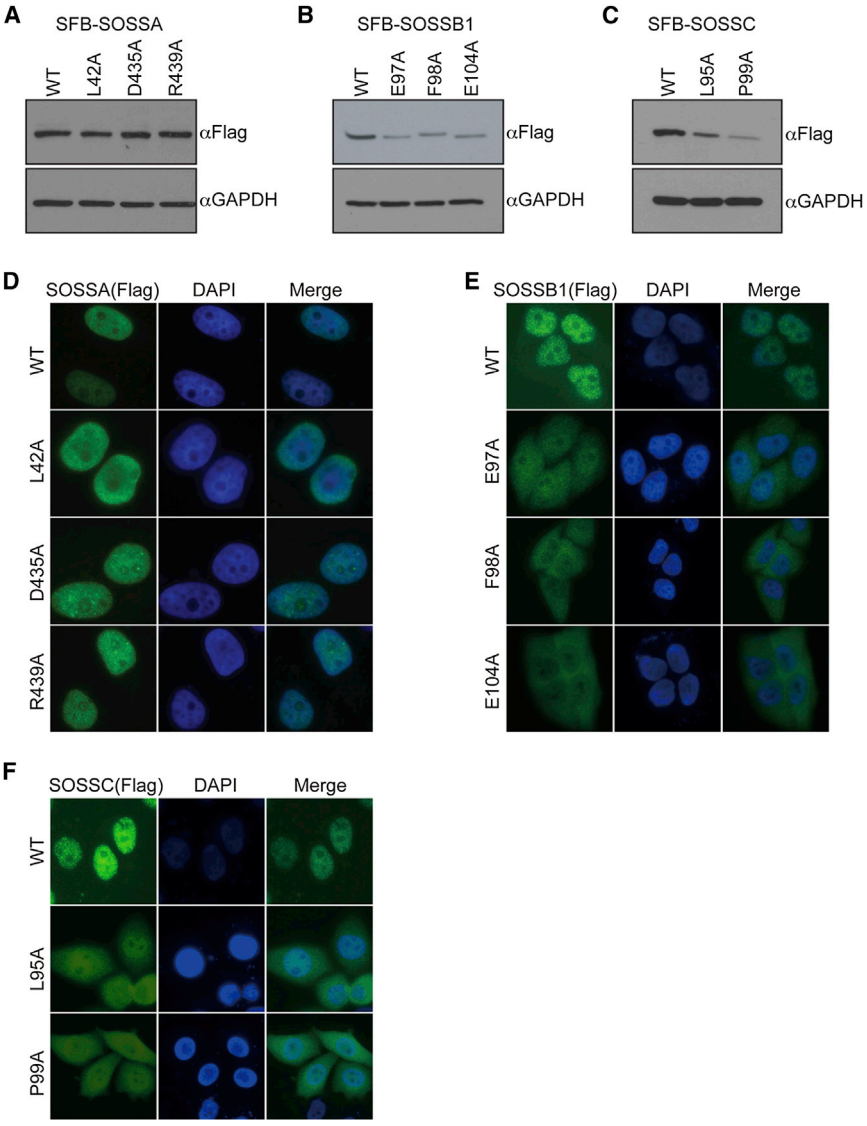

Figure 3. SOSSA Regulates SOSSB1/SOSSC Stability and Nuclear Localization

(A–C) SOSSA regulates SOSSB1/SOSSC stability. Cells to express wild-type SOSSB1/SOSSC (SiR-WT) or their point mutants defective in SOSSA binding (L95A, P99A, E97A, F98A, and E104A) under the control of a tetracycline-inducible promoter were generated. After 24 hr of doxycycline (1 μg/ml) induction, the cells were collected, and whole-cell lysates were probed with the indicated antibodies.

(D–F) SOSSA controls the SOSSB1/SOSSC nuclear localization. Cells to express wild-type SOSSB1/SOSSC (WT) or their point mutants defective in SOSSA binding (L95A, P99A, E97A, F98A, and E104A) under the control of a tetracycline-inducible promoter were generated. Cells were induced by doxycycline addition for 24 hr before fixing and processed for immunofluorescence.

in the $SOSSA_N$/B1/dT12 complex. For simplicity, we have numbered nucleotides T1 to T9 in the 5′→3′ direction. SOSS1 has been shown to bind ssDNA with a minimal length of 35 nt (Yang et al., 2013). To investigate how SOSS1 recognize longer ssDNA, we determined the crystal structure of $SOSSA_N$/B1/C in complex with 35 nucleotide poly(dT) (designated as $SOSSA_N$/B1/C/dT35). Unexpectedly, of the 35 nt poly(dT) used in crystallization, only six moderately ordered deoxythymidine nucleotides were observed in $SOSSA_N$/B1/C/dT35. As shown in Figures 1D and 1E, the ssDNA in both structures adopts an extended conformation and interacts exclusively with SOSSB1. SOSSC is not involved in ssDNA binding in the $SOSSA_N$/B1/C/dT35 complex (Figure 1E). $SOSSA_N$ in the structures of both $SOSSA_N$/B1/dT12 and $SOSSA_N$/B1/C/dT35 interacts with ssDNA through a symmetry-related molecule within the crystal lattice. However, mutations of residues of $SOSSA_N$ predicted to be involved in ssDNA binding have little or no effects on the DNA binding activity of $SOSSA_N$/B1/C (Figure S4), suggesting that $SOSSA_N$ might not be involved in ssDNA binding and the contacts between $SOSSA_N$ and ssDNA are created by the crystal packing forces. Because the ssDNA binds to SOSSB1 in both structures with a similar conformation, for simplicity, only the 9 nt poly(dT) and its interactions with the SOSS1 subunits in the $SOSSA_N$/B1/dT12 complex are analyzed subsequently.

In the structures of both $SOSSA_N$/B1/dT12 and $SOSSA_N$/B1/C/dT35, SOSSB1 interacts with SOSSA and ssDNA via distinct surfaces. Specifically, SOSSB1 interacts with ssDNA via a groove formed by residues 12–16 in the N terminus, loops $\beta2_B$-$\beta3_B$ and $\beta4_B$-$\alpha1_B$, and strands $\beta4_B$, $\beta5_B$, and $\beta6_B$, whereas SOSSB1 interacts with SOSSA through strand $\beta1_B$, $\beta6_B$, helix $\alpha1_B$, the $\alpha1_B$-$\beta5_B$ loop, and its C-terminal tail (Figures 1D and 1E). Consistent with this observation, immunoprecipitation combined with mutagenesis showed that the OB fold domain of SOSSB1 is required for both ssDNA binding and interaction with SOSSA (previously named as INTS3) (Gu et al., 2013; Skaar et al., 2009).

Recognition of ssDNA

In the structure of the $SOSSA_N$/B1/dT12 complex, the bound ssDNA displays an extended conformation with a U-shaped bend between T5 and T6, such that the thymine base of T5 points in the direction opposite to those of T4 and T6 (Figure 5A). The binding of ssDNA to SOSSB1 is mediated mainly by a combination of electrostatic and hydrogen-bonding and base-staking interactions as depicted in Figure 5A.

Briefly, T1 and T2 at the 5′ end and T8 and T9 the 3′ end of dT12 are largely exposed to the solvent region with only one

water-mediated contact formed between the O2 atom of the T8 base and Lys33$_B$ of SOSSB1. The N3 atom of the T3 base is hydrogen bonded to the carboxyl group of Asp56$_B$ of SOSSB1, whereas the O1P atoms of both T4 and T5 contact the side chain of Arg88$_B$ of SOSSB1 through electrostatic interactions. The base of T5 lies on the DNA binding groove of SOSSB1, and its N3 atom is hydrogen bonded to the main-chain carbonyl group of Gly13$_B$. The thymine bases of T6 and T7 stack against the indole group of Trp55$_B$ and the benzyl group of Phe78$_B$, respectively, whereas the O4 atom of the T7 base forms a hydrogen bond with the hydroxyl group of Tyr85$_B$.

To examine the role of the residues involved in multiple contacts with ssDNA biochemically, we mutated several residues and examined the mutational effects on ssDNA binding by electrophoretic mobility shift assay (EMSA). As shown in Figure 5B, mutations of Trp55$_B$ and Phe78$_B$ to Ala, which are involved in stacking interactions with the bases of T6 and T7, reduced DNA binding substantially. In support of our observations, mutation of Trp55 (equivalent to Trp55 in human SOSSB1) to Ala significantly reduced the ssDNA binding of mouse SSB1 (Gu et al., 2013). Consistent with these observations, the W55A and F78A mutants still bound SOSSA (Figure 2E) but failed to rescue RAD51 foci formation in SOSSB1-depleted cells (Figures 4B and S3). These results reinforce the notion that SOSSB1 interacts with SOSSA and ssDNA through distinct surface regions and suggest that the binding of SOSSB1 to ssDNA is critical for DNA repair.

SOSSC and SOSSA$_N$ Are Not Required for ssDNA Binding

Purified human SSB1 has been shown to bind ssDNA with the binding affinity increased significantly with the length of the ssDNA substrate (Richard et al., 2008). Moreover, the SOSS1 complex has been reported to recognize the minimal ~35 nt ssDNA (Yang et al., 2013), which is in contrast with the 10 nt minimal binding site reported for RPA (Fanning et al., 2006). However, our structures showed that both SOSSA$_N$/B1 and SOSSA$_N$/B1/C are capable of binding ssDNA with minimal length of ~10 nt. Furthermore, the role of SOSSC in ssDNA binding is not clear as most nucleotides of the 35 nt ssDNA used for cocrystallization are disordered in our structure.

To further examine the effect of SOSSC and SOSSA$_N$ on the ssDNA binding of SOSS1, isothermal titration calorimetry (ITC) was used to titrate dT12 or dT48 to SOSSB1 alone, SOSSA$_N$/B1, and SOSSA$_N$/B1/C. As shown in Figure S5, SOSSB1, SOSSA$_N$/B1, and SOSSA$_N$/B1/C showed comparable binding affinities to dT12. Similarly, SOSSB1, SOSSA$_N$/B1, and SOSSA$_N$/B1/C also exhibited comparable binding affinities to dT48 (Figure S5), although the K_d values are five to eight times lower compared to those of the titrations by dT12. These results suggest that SOSSC and SOSSA$_N$ are not critical for ssDNA binding regardless of the ssDNA length.

DISCUSSION

Several lines of evidence suggest that RPA and SOSS1 may have different affinities and specificities for DNA substrates. First, RPA has essential activities in DNA replication besides its role in DNA repair (Iftode et al., 1999; Wold, 1997; Zou et al., 2006), whereas the functions of the SOSS1 complex are limited to repair and signaling that occurs at DSBs (Huang et al., 2009; Li et al., 2009; Skaar et al., 2009). Second, RPA and SOSS1 do not exhibit colocalization, albeit they both are recruited to the sites of DSBs (Huang et al., 2009). Third, SOSS1 contains only a single OB fold domain, whereas RPA has six OB fold domains, four of which bind ssDNA (Fan and Pavletich, 2012; Huang et al., 2009). Consequently, SOSS1 binds ssDNA with much lower affinity compared to RPA (Yang et al., 2013). Moreover, RPA binds to ssDNA in at least two conformational states with opposing affinities, depending on the length of ssDNA (Fan and Pavletich, 2012; Fanning et al., 2006), whereas SOSS1 appears to have a single conformational state wherein one SOSS1 complex binds to the ssDNA, forming a less stable and dynamic complex (Yang et al., 2013).

Our crystal structures showed that the SOSSA$_N$/B1/C complex binds to a 35 nt ssDNA, occluding a region of 6 nt with the rest of the ssDNA disordered, whereas the SOSSA$_N$/B1/dT12 complex binds nine ordered nucleotides. Our ITC data indicated that both SOSSA$_N$/B1 and SOSSA$_N$/B1/C bind a 12 nt ssDNA with comparable affinities. These observations show that SOSS1, like RPA, is capable of binding a short ssDNA, in contrast to the previous report showing that the minimal length of ssDNA required for SOSS1 binding is ~35 nt (Yang et al., 2013). Although SOSS1 has been shown to bind to ssDNA with an affinity of at least 30-fold higher than that reported for SOSSB1 alone (Richard et al., 2008; Yang et al., 2013), our ITC results showed that SOSSB1 alone, SOSSA$_N$/B1 and SOSSA$_N$/B1/C exhibited comparable binding affinities toward ssDNA. Given that SOSSA$_N$ and SOSSC are not involved in ssDNA binding and the SOSS1 complex is capable of recognizing a minimal 35 nt ssDNA, recognition of longer ssDNA might be conferred by the C-terminal half of SOSSA, whereas the role of SOSSA$_N$ is just to bridge the interactions of SOSSB1 and SOSSC for the SOSS1 complex assembly. However, the C-terminal half of SOSSA has been reported to be required for binding INST6 in the hSSB1-INTS complex (Zhang et al., 2013). Further structural studies are required to clarify the role of the C-terminal half of SOSSA in the DNA damage response.

SOSS1 has been reported to stimulate the exo- and endonuclease activities of hExo1 on DNA by promoting hExo1 recruitment to DNA ends, thereby leading to an increased activity of hExo1 at DSBs (Yang et al., 2013). Although SOSS1 and hExo1 bind to dsDNA substrates cooperatively in vitro, no direct interaction between SOSS1 and hExo1 has been observed. Therefore, SOSS1 has been proposed to stimulate the recruitment of hExo1 to DSBs by stabilizing an opened or Y-shaped duplex at DNA ends. Consistent with this view, hExo1 preferentially binds to a Y-shaped duplex over a fully paired duplex (Yang et al., 2013). The crystal structure of hExo1 in complex with a DNA substrate containing a short 3′ ssDNA overhang showed that hExo1 induces a sharp bend of the 3′ complementary DNA strand for nick or gap recognition (Orans et al., 2011). The frayed 5′ ends of nicked duplexes resemble flap junctions, hence unifying the mechanism of exo- and endonuclease activities of hExo1. Our structure showed that SOSS1 is able to recognize a short ssDNA. It is envisaged that SOSS1 could promote and/or stabilize the frayed 5′ ends of nicked dsDNA through the

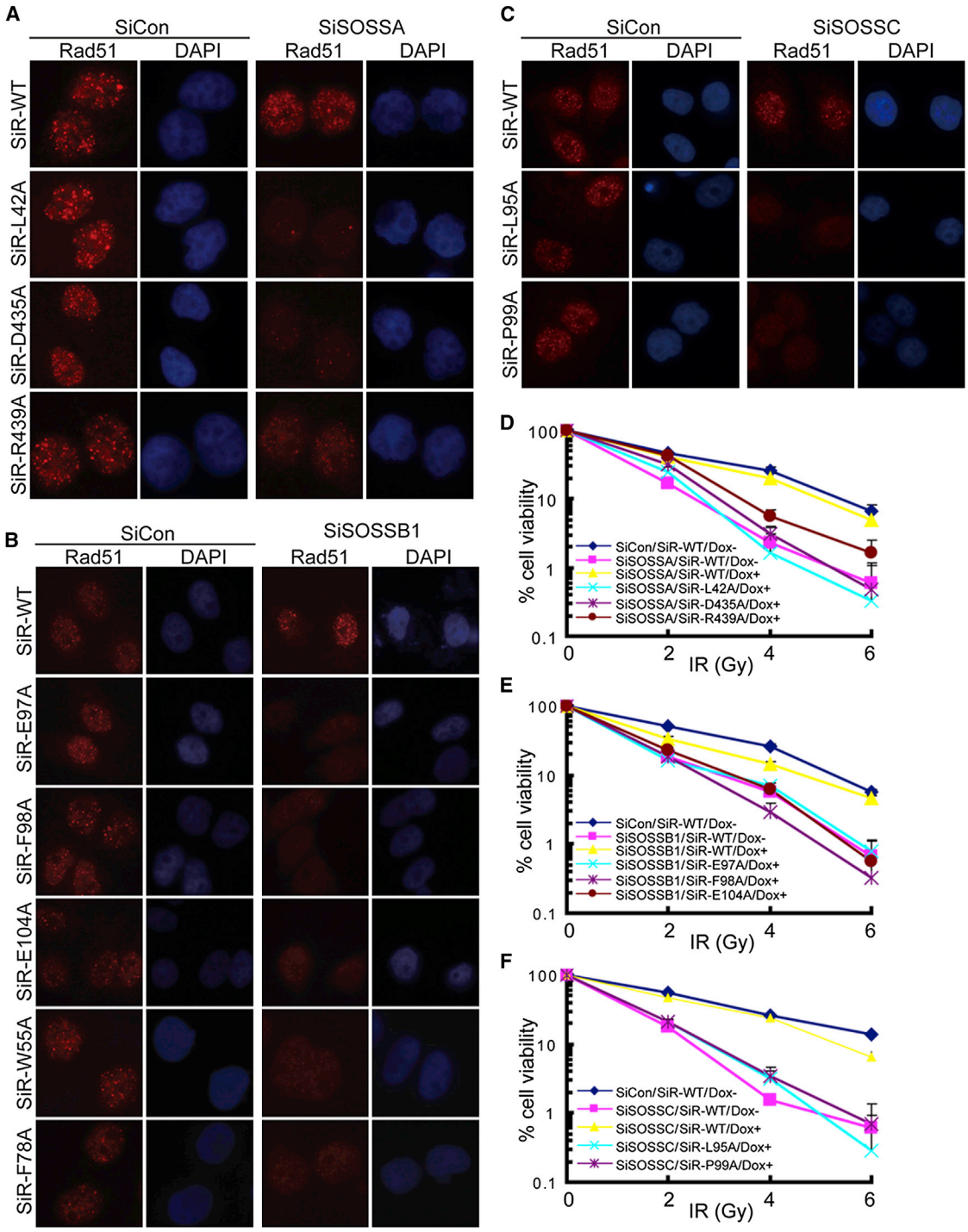

Figure 4. The Assembly of the SOSS1 Complex Is Necessary for Proper DNA Repair

(A) Cells that express siRNA#1-resistant wild-type SOSSA (SiR-WT) or its point mutants defective in SOSSB1 or SOSSC binding (SiR-L42A, SiR-D435A, and SiR-R439A) under the control of a tetracycline-inducible promoter were generated. The resulting cell lines were transfected twice with SOSSA siRNA. Twenty-four hours after the second transfection, cells were induced by doxycycline addition for 24 hr prior to IR (10 Gy) treatment. Six hours later, cells were fixed and processed for RAD51 immunofluorescence.

(B) Cells that express siRNA#1-resistant wild-type SOSSB1 (SiR-WT) or its point mutants (SiR-W55A, SiR-F78A, SiR-E97A, SiR-F98A, and SiR-E104A) under the control of a tetracycline-inducible promoter were generated. The resulting cell lines were transfected twice with SOSSB1 siRNA. Twenty-four hours after the second transfection, cells were induced by doxycycline addition for 24 hr prior to IR (10 Gy) treatment. Six hours later, cells were fixed and processed for RAD51 immunofluorescence. More than one hundred cells were counted in each experiment.

(legend continued on next page)

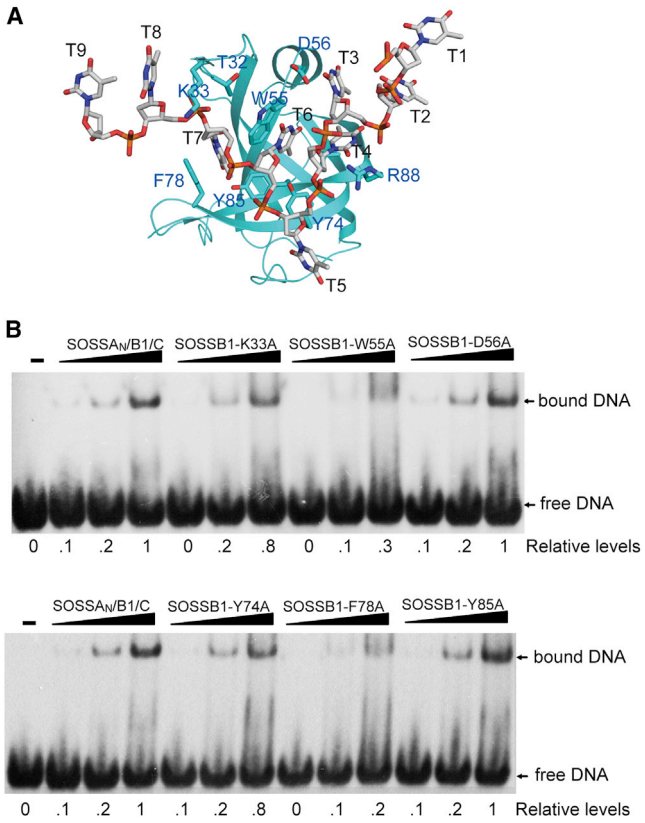

Figure 5. The Interaction of SOSSB1 with ssDNA

(A) The bound ssDNA and the residues involved in the SOSSB1-DNA interactions are shown in stick models. The color scheme of protein is as in Figure 1, and the DNA is in gray.

(B) Mutational effects of SOSSB1 on the binding to dT48 examined by the electrophoretic mobility shift assay (EMSA). The mutant $SOSSA_N$/B1/C complexes were reconstituted by mixing the SOSSB1 mutants with corresponding wild-type SOSS subunits and incubating on ice for 1 hr before loading to the gel. The amount of DNA shifted were quantified and normalized against the total DNA shifted by wild-type $SOSSA_N$/B1/C complex at the highest concentration.

binding of SOSSB1 to this 3′ ssDNA overhang, thereby facilitating 5′ strand resection of DSBs.

SOSS1 is also reported to bind the MRN complex, but the subunits involved in SOSS1-MRN interaction and the order of recruitment of SOSS1 and MRN to the sites of DSBs remain controversial. Previously, we showed that SOSSA specifically interacts with the NBS1 subunit of the MRN complex (Huang et al., 2009). This, together with the observation that MRN is required for SOSS foci formation in S/G2 cells, suggests that SOSS1 functions downstream of the MRN complex with SOSSA facilitating the recruitment of SOSS1 to the DNA damaging sites.

Recently, SOSSB1 was reported to rapidly bind at the sites of DSBs and was required for the efficient recruitment of the MRN complex (Richard et al., 2011b). As SOSSB1 is one of the subunits of the SOSS1 complex, this result suggests that SOSS1 functions upstream of the MRN complex. Further biochemical studies showed that SOSSB1 directly interacts with the MRN complex, and this interaction is mediated by the C-terminal tail of SOSSB1 and the N terminus of NBS1 (Richard et al., 2011a). This direct interaction was further shown to be required for SOSSB1 stimulating the endonuclease activity of the MRN complex (Richard et al., 2011a). However, in contrast to this report, Yang and his colleagues did not observe any stimulation of MRN nuclease activity by SOSS1 (Yang et al., 2013). Clearly, more studies are needed to define the exact role of SOSS1 in DSB repair. One of the future important goals is to elucidate the mechanism by which SOSS1 interacts with the MRN complex and Exo1 at the sites of DSBs, thus promoting DSB resection.

EXPERIMENTAL PROCEDURES

Details of protein expression, purification, and crystallization are described in the Supplemental Experimental Procedures. Diffraction data were collected at the peak wavelength of selenium absorption edge (λ = 0.9798 Å) at beamline BL17U, Shanghai Synchrotron Radiation facility (SSRF), China. The data sets were integrated using MOSFLM (Leslie, 2006). Scaling of intensities was carried out using SCALA from the CCP4i package (Potterton et al., 2003). The crystals of apo $SOSS_N$/A/B1/C belong to space group $P3_121$ with one molecule in the asymmetric unit (AU). Fifteen out of 17 Se sites were found by Autosol in the PHENIX software suite (Adams et al., 2010). Automatic partial model building was carried out by AutoBuild in the PHENIX software suite (Adams et al., 2010). The model was further built manually using COOT (Emsley and Cowtan, 2004). Crystallographic refinement was performed using the PHENIX software suite (Adams et al., 2010). Water molecules were added using Arp/Warp solvent (Perrakis et al., 2001). The final model has good stereochemistry with a free R factor of 19.53% and an R factor of 17.19%.

The structures of $SOSSA_N$/B1/C/dT35 and $SOSSA_N$/B1/dT12 were solved using molecular replacement with PHASER (McCoy et al., 2007), using $SOSSA_N$/B1/C and $SOSSA_N$/B1 as the search models respectively. Model refinement was carried out with the PHENIX software. DNA molecules were included in the final stages of refinement. Difference Fourier maps clearly showed the electron density for six and nine deoxyribonucleotides for $SOSSA_N$/B1/C/dT35 and $SOSSA_N$/B1/dT12, respectively. The stereochemical geometry of the structures was validated using PROCHECK (Laskowski et al., 1993). The statistics for data collection and refinement and the quality of the final models are summarized in Table S1.

Immunofluorescence Staining

Indirect immunofluorescence was carried out as described (Huang et al., 2009). HeLa cells cultured on coverslips were treated with IR (10 Gy) for 6 hr. Cells were then washed with PBS, pre-extracted with buffer containing 0.5% Triton X-100 for 5 min, and fixed with 3% paraformaldehyde for 10 min at room temperature. Cells were incubated in primary antibody for 30 min at room temperature. After three 5 min washes with PBS, secondary antibody was added and incubated at room temperature for 30 min. Cells were then

(C) Cells that express siRNA#1-resistant wild-type SOSSC (SiR-WT) or its point mutants defective in SOSSA binding (SiR-L95A and SiR-P99A) under the control of a tetracycline-inducible promoter were generated. Immunofluorescence staining was performed similar to those described in (A).

(D–F) Cells that express siRNA-resistant wild-type SOSSA/SOSSB1/SOSSC or their point mutants under the control of a tetracycline-inducible promoter were generated. The resulting cell lines were transfected twice with control or SOSSA/SOSSB1/SOSSC siRNAs. Following IR treatment, cells were permitted to grow for 14 days before staining. Experiments were done in triplicates. Results shown are averages of three independent experiments.

stained with DAPI to visualize nuclear DNA. The coverslips were mounted onto glass slides with antifade solution and visualized using a Nikon ECLIPSE i80 fluorescence microscope with a Nikon Plan Fluor 60× oil objective lens.

ACCESSION NUMBERS

The coordinates and structure-factor amplitudes of $SOSSA_N$/B1/C, $SOSSA_N$/B1/C/dT35, and $SOSSA_N$/B1/dT12 have been deposited in the Protein Data Bank with accession codes 4OWT, 4OWW, and 4OWX, respectively.

SUPPLEMENTAL INFORMATION

Supplemental Information includes Supplemental Experimental Procedures, five figures, and one table and can be found with this article online at http://dx.doi.org/10.1016/j.celrep.2014.02.020.

ACKNOWLEDGMENTS

We would like to thank the beamline scientists at BL17U, Shanghai Synchrotron Radiation facility (SSRF), China for assistance and access to synchrotron radiation facilities. This work was supported by Natural Science Foundation of China (grant no. 31270816; to H.S.) and the Agency for Science, Technology and Research in Singapore (to H.S.) and by National Program for Special Support of Eminent Professionals, National Basic Research Program of China Grants 2012CB944402 and 2013CB911003, National Natural Science Funds for Distinguished Young Scholar, National Natural Science Foundation of China Grant 31071243, and Zhejiang University K.P. Chao's High Technology Development Foundation (to J.H.).

Received: January 3, 2014
Revised: February 6, 2014
Accepted: February 14, 2014
Published: March 13, 2014

REFERENCES

Adams, P.D., Afonine, P.V., Bunkóczi, G., Chen, V.B., Davis, I.W., Echols, N., Headd, J.J., Hung, L.W., Kapral, G.J., Grosse-Kunstleve, R.W., et al. (2010). PHENIX: a comprehensive Python-based system for macromolecular structure solution. Acta Crystallogr. D Biol. Crystallogr. *66*, 213–221.

Aguilera, A., and Gómez-González, B. (2008). Genome instability: a mechanistic view of its causes and consequences. Nat. Rev. Genet. *9*, 204–217.

Bartek, J., Lukas, C., and Lukas, J. (2004). Checking on DNA damage in S phase. Nat. Rev. Mol. Cell Biol. *5*, 792–804.

D'Amours, D., and Jackson, S.P. (2002). The Mre11 complex: at the crossroads of dna repair and checkpoint signalling. Nat. Rev. Mol. Cell Biol. *3*, 317–327.

Emsley, P., and Cowtan, K. (2004). Coot: model-building tools for molecular graphics. Acta Crystallogr. D Biol. Crystallogr. *60*, 2126–2132.

Fan, J., and Pavletich, N.P. (2012). Structure and conformational change of a replication protein A heterotrimer bound to ssDNA. Genes Dev. *26*, 2337–2347.

Fanning, E., Klimovich, V., and Nager, A.R. (2006). A dynamic model for replication protein A (RPA) function in DNA processing pathways. Nucleic Acids Res. *34*, 4126–4137.

Flynn, R.L., and Zou, L. (2010). Oligonucleotide/oligosaccharide-binding fold proteins: a growing family of genome guardians. Crit. Rev. Biochem. Mol. Biol. *45*, 266–275.

Gu, P., Deng, W., Lei, M., and Chang, S. (2013). Single strand DNA binding proteins 1 and 2 protect newly replicated telomeres. Cell Res. *23*, 705–719.

Holm, L., and Rosenström, P. (2010). Dali server: conservation mapping in 3D. Nucleic Acids Res. *38* (Web Server issue), W545–W549.

Huang, J., Gong, Z., Ghosal, G., and Chen, J. (2009). SOSS complexes participate in the maintenance of genomic stability. Mol. Cell *35*, 384–393.

Iftode, C., Daniely, Y., and Borowiec, J.A. (1999). Replication protein A (RPA): the eukaryotic SSB. Crit. Rev. Biochem. Mol. Biol. *34*, 141–180.

Jackson, S.P., and Bartek, J. (2009). The DNA-damage response in human biology and disease. Nature *461*, 1071–1078.

Jazayeri, A., Balestrini, A., Garner, E., Haber, J.E., and Costanzo, V. (2008). Mre11-Rad50-Nbs1-dependent processing of DNA breaks generates oligonucleotides that stimulate ATM activity. EMBO J. *27*, 1953–1962.

Kerr, I.D., Wadsworth, R.I., Cubeddu, L., Blankenfeldt, W., Naismith, J.H., and White, M.F. (2003). Insights into ssDNA recognition by the OB fold from a structural and thermodynamic study of Sulfolobus SSB protein. EMBO J. *22*, 2561–2570.

Laskowski, R.A., MacArthur, M.W., Moss, D.S., and Thornton, J.M. (1993). PROCHECK: a program to check the stereochemical quality of protein structures. J. Appl. Cryst. *26*, 283.

Lee, J.H., and Paull, T.T. (2005). ATM activation by DNA double-strand breaks through the Mre11-Rad50-Nbs1 complex. Science *308*, 551–554.

Lei, J., Mesters, J.R., von Brunn, A., and Hilgenfeld, R. (2011). Crystal structure of the middle domain of human poly(A)-binding protein-interacting protein 1. Biochem. Biophys. Res. Commun. *408*, 680–685.

Leslie, A.G. (2006). The integration of macromolecular diffraction data. Acta Crystallogr. D Biol. Crystallogr. *62*, 48–57.

Li, Y., Bolderson, E., Kumar, R., Muniandy, P.A., Xue, Y., Richard, D.J., Seidman, M., Pandita, T.K., Khanna, K.K., and Wang, W. (2009). HSSB1 and hSSB2 form similar multiprotein complexes that participate in DNA damage response. J. Biol. Chem. *284*, 23525–23531.

McCoy, A.J., Grosse-Kunstleve, R.W., Adams, P.D., Winn, M.D., Storoni, L.C., and Read, R.J. (2007). Phaser crystallographic software. J. Appl. Cryst. *40*, 658–674.

McKinnon, P.J. (2009). DNA repair deficiency and neurological disease. Nat. Rev. Neurosci. *10*, 100–112.

Morino, S., Imataka, H., Svitkin, Y.V., Pestova, T.V., and Sonenberg, N. (2000). Eukaryotic translation initiation factor 4E (eIF4E) binding site and the middle one-third of eIF4GI constitute the core domain for cap-dependent translation, and the C-terminal one-third functions as a modulatory region. Mol. Cell. Biol. *20*, 468–477.

Murzin, A.G. (1993). OB(oligonucleotide/oligosaccharide binding)-fold: common structural and functional solution for non-homologous sequences. EMBO J. *12*, 861–867.

Orans, J., McSweeney, E.A., Iyer, R.R., Hast, M.A., Hellinga, H.W., Modrich, P., and Beese, L.S. (2011). Structures of human exonuclease 1 DNA complexes suggest a unified mechanism for nuclease family. Cell *145*, 212–223.

Perrakis, A., Harkiolaki, M., Wilson, K.S., and Lamzin, V.S. (2001). ARP/wARP and molecular replacement. Acta Crystallogr. D Biol. Crystallogr. *57*, 1445–1450.

Potterton, E., Briggs, P., Turkenburg, M., and Dodson, E. (2003). A graphical user interface to the CCP4 program suite. Acta Crystallogr. D Biol. Crystallogr. *59*, 1131–1137.

Richard, D.J., Bolderson, E., Cubeddu, L., Wadsworth, R.I., Savage, K., Sharma, G.G., Nicolette, M.L., Tsvetanov, S., McIlwraith, M.J., Pandita, R.K., et al. (2008). Single-stranded DNA-binding protein hSSB1 is critical for genomic stability. Nature *453*, 677–681.

Richard, D.J., Cubeddu, L., Urquhart, A.J., Bain, A., Bolderson, E., Menon, D., White, M.F., and Khanna, K.K. (2011a). hSSB1 interacts directly with the MRN complex stimulating its recruitment to DNA double-strand breaks and its endo-nuclease activity. Nucleic Acids Res. *39*, 3643–3651.

Richard, D.J., Savage, K., Bolderson, E., Cubeddu, L., So, S., Ghita, M., Chen, D.J., White, M.F., Richard, K., Prise, K.M., et al. (2011b). hSSB1 rapidly binds at the sites of DNA double-strand breaks and is required for the efficient recruitment of the MRN complex. Nucleic Acids Res. *39*, 1692–1702.

Shereda, R.D., Kozlov, A.G., Lohman, T.M., Cox, M.M., and Keck, J.L. (2008). SSB as an organizer/mobilizer of genome maintenance complexes. Crit. Rev. Biochem. Mol. Biol. *43*, 289–318.

Skaar, J.R., Richard, D.J., Saraf, A., Toschi, A., Bolderson, E., Florens, L., Washburn, M.P., Khanna, K.K., and Pagano, M. (2009). INTS3 controls the hSSB1-mediated DNA damage response. J. Cell Biol. *187*, 25–32.

Sonoda, E., Hochegger, H., Saberi, A., Taniguchi, Y., and Takeda, S. (2006). Differential usage of non-homologous end-joining and homologous recombination in double strand break repair. DNA Repair (Amst.) *5*, 1021–1029.

Symington, L.S., and Gautier, J. (2011). Double-strand break end resection and repair pathway choice. Annu. Rev. Genet. *45*, 247–271.

Tran, P.T., Erdeniz, N., Symington, L.S., and Liskay, R.M. (2004). EXO1-A multi-tasking eukaryotic nuclease. DNA Repair (Amst.) *3*, 1549–1559.

Wold, M.S. (1997). Replication protein A: a heterotrimeric, single-stranded DNA-binding protein required for eukaryotic DNA metabolism. Annu. Rev. Biochem. *66*, 61–92.

Xu, S., Feng, Z., Zhang, M., Wu, Y., Sang, Y., Xu, H., Lv, X., Hu, K., Cao, J., Zhang, R., et al. (2011). hSSB1 binds and protects p21 from ubiquitin-mediated degradation and positively correlates with p21 in human hepatocellular carcinomas. Oncogene *30*, 2219–2229.

Xu, S., Wu, Y., Chen, Q., Cao, J., Hu, K., Tang, J., Sang, Y., Lai, F., Wang, L., Zhang, R., et al. (2013). hSSB1 regulates both the stability and the transcriptional activity of p53. Cell Res. *23*, 423–435.

Yang, S.H., Zhou, R., Campbell, J., Chen, J., Ha, T., and Paull, T.T. (2013). The SOSS1 single-stranded DNA binding complex promotes DNA end resection in concert with Exo1. EMBO J. *32*, 126–139.

Zhang, F., Wu, J., and Yu, X. (2009). Integrator3, a partner of single-stranded DNA-binding protein 1, participates in the DNA damage response. J. Biol. Chem. *284*, 30408–30415.

Zhang, F., Ma, T., and Yu, X. (2013). A core hSSB1-INTS complex participates in the DNA damage response. J. Cell Sci. *126*, 4850–4855.

Zou, Y., Liu, Y., Wu, X., and Shell, S.M. (2006). Functions of human replication protein A (RPA): from DNA replication to DNA damage and stress responses. J. Cell. Physiol. *208*, 267–273.